THE JOURNAL OF COMPARATIVE NEUROLOGY 466:343–355 (2003)

Dopaminergic Amacrine Cells in the Inner Nuclear Layer and Ganglion Cell Layer Comprise a Single Functional Retinal Mosaic

STEPHEN J. EGLEN,[1]* MARY A. RAVEN,[2] ERIC TAMRAZIAN,[2] AND BENJAMIN E. REESE[2]

[1]Department of Anatomy and Neurobiology, Washington University School of Medicine, St. Louis, Missouri 63110

[2]Neuroscience Research Institute and Department of Psychology, University of California at Santa Barbara, Santa Barbara, California 93106

ABSTRACT

Many types of retinal neuron are distributed in an orderly manner across the surface of the retina. Indeed, the existence of such regularity amongst a population of neurons, termed a retinal mosaic, may be a defining feature of functionally independent types of retinal neuron. We have examined the spatial distribution of dopaminergic amacrine cells in the ferret retina both in the inner nuclear layer (INL) and in the ganglion cell layer (GCL) to determine whether the cells in each layer form an independent retinal mosaic as evidence of whether they should be considered as two separate types. Ferret retinas contain approximately 1,900 dopaminergic amacrine cells, of which 27% are located in the GCL, and the rest in the INL. Based on analysis of their Voronoi domains as well as autocorrelation analysis and tests for complete spatial randomness, we found that the distribution of INL cells was statistically regular, while that of the GCL cells was not. However, by using cross-correlation analysis, these two groups of cells were found to be spatially dependent: an exclusion zone was detected in the cross-correlogram of roughly the same size as that found in the autocorrelograms of both INL and GCL cells. Such a pattern would be expected if dopaminergic amacrine cells in the INL and GCL were members of a single regular population differing only in their somatic depth. By using computer simulations, we tested this hypothesis directly, confirming that a random assignment of 27% from the total population produces cross-correlograms that are indistinguishable from those of the biological mosaics. We conclude, therefore, that the cells in the two layers form a single functional population; those in the GCL appear to be misplaced. Somatic positioning with respect to depth within the retina is not, by itself, a reliable guide for functional classification. J. Comp. Neurol. 466:343–355, 2003.

Indexing terms: tyrosine hydroxylase; nearest neighbor; Voronoi domain; autocorrelation; cross-correlation; density recovery profile

Retinal nerve cells are commonly arranged as orderly mosaics, in which the individual cells of a particular type are distributed as nonrandom arrays, ensuring a uniform sampling of the visual field. Indeed, the presence of such regularity in a population of retinal neurons has been considered a defining feature of a functional class of cell (Cook, 1996, 1998). Dopaminergic amacrine cells are one of the most sparsely distributed retinal nerve cell types found within the mammalian retina (Brecha et al., 1984; Mariani et al., 1984; Versaux-Botteri et al., 1984; Mitrofanis et al., 1988; Savy et al., 1989; Wulle and Schnitzer,

Grant sponsor: Wellcome Trust; Grant number: 061797; Grant sponsor: National Institutes of Health; Grant number: EY-11087.

*Correspondence to: Stephen J. Eglen, Institute for Adaptive and Neural Computation, School of Informatics, University of Edinburgh, 5 Forrest Hill, Edinburgh, EH1 2QL, U.K. E-mail: stephen@inf.ed.ac.uk

Received 2 May 2003; Revised 16 June 2003; Accepted 16 June 2003

DOI 10.1002/cne.10891

Published online the week of September 29, 2003 in Wiley InterScience (www.interscience.wiley.com).

1989; Dacey, 1990; Müller and Peichl, 1991; Peichl, 1991), yet there is little agreement on the spatial patterning within this mosaic. Even within the same species, different investigators have described their distribution as being "randomly distributed" (Versaux-Botteri et al., 1984), "irregular" (Gustincich et al., 1997), or "regularly ordered" (Wulle and Schnitzer, 1989). Others report the mosaic as being "neither a random nor a highly regular pattern" (Brecha et al., 1984). The questionable regularity of this population of cells is understandable; unlike other cell types that are arranged in a regular array to faithfully encode and transmit the visual scene (e.g., on-center beta retinal ganglion cells), the dopaminergic amacrine cells play a modulatory role in the processing of signals (Daw et al., 1990; Xin and Bloomfield, 1999; Weiler et al., 2000), consistent with their extrasynaptic release of dopamine and the widespread distribution of dopamine receptors (Veruki and Wässle, 1996; Nguyen-Legros et al., 1999; Puopolo et al., 2001).

In some species, several of the dopaminergic amacrine cells are situated within the ganglion cell layer (GCL) rather than within the inner nuclear layer (INL), but they are similar with respect to soma size, and they arborize in the same stratum of the inner plexiform layer (IPL), suggesting that cells in both retinal layers comprise a single functional population (Oyster et al., 1985; Kolb et al., 1990; Peichl, 1991). This arrangement is to be contrasted with the cholinergic amacrine cells: these cells are also situated in either the GCL or the INL, they have comparable morphologies, and usually have similar soma size distributions. Unlike the dopaminergic amacrine cells, however, these two populations arborize in distinct sublaminae within the IPL where they participate in functionally distinct ON and OFF visual pathways (Masland and Mills, 1979; Schmidt et al., 1985; Pourcho and Osman, 1986; Famiglietti and Tumosa, 1987; Brandon, 1987; Rodieck and Marshak, 1992). In the absence of any data directly addressing the functional contributions of the dopaminergic amacrine cells in the INL and GCL, one cannot be sure that, despite their similar pharmacological and anatomical signatures within the IPL, they are not functionally independent cell types.

One approach to this problem is to consider the spatial relationships between these cells. If the cells in the INL and GCL comprise a single functional type, then there should be a spatial dependency between their positioning in the plane of the retina, and their combined population should create a more regular mosaic than either alone. By contrast, the cholinergic amacrine cells in the INL and GCL are spatially independent of one another, and the mosaic regularity of either population is greater than the combined population (Vaney et al., 1981; Diggle, 1986; Voigt, 1986; Rockhill et al., 2000; Eglen and Willshaw, 2002), consistent with their being functionally distinct populations. To date, however, the spatial distributions of dopaminergic amacrine cells in the INL and GCL have not been quantitatively examined to test whether the cells form a single population or two populations.

In this study, we use several statistical techniques to investigate the spatial distribution of dopaminergic amacrine cells in the INL and GCL. To establish the regularity of each population of dopaminergic amacrine cells compared with other populations of retinal cells, we calculated regularity indexes based on the distribution of both nearest-neighbor distances and Voronoi domain areas. In addition, we used statistical tests to determine whether the INL or GCL cells are discriminable from random distributions (Diggle, 1986). To address the issue of whether cells in the INL and GCL are two separate populations or just one population, we used two related techniques, based on spatial cross-correlations between cells. First, we used a test of spatial dependence to ask whether there is any particular spatial relationship between the cells in the INL and GCL. Second, we tested whether the positioning of amacrine cells in the INL vs. GCL was decided at random. Our results demonstrate that the dopaminergic amacrine cells in the INL and GCL form a single retinal mosaic, indicating that the two cells belong to the same type.

MATERIALS AND METHODS

Tissue preparation and data acquisition

Ten adult female ferrets (*Mustela putorius furo*) obtained from Marshall Research Animals (North Rose, NY) were sedated with an intramuscular injection of ketamine (10 mg/kg) and xylazine (1 mg/kg) and subsequently anesthetized with a lethal dose of sodium pentobarbital injected intraperitoneally (120 mg/kg). Ferrets were perfused transcardially with 200 ml of 0.9% saline followed by 1 liter of 4% paraformaldehyde in 0.1 M sodium phosphate buffer (pH 7.2 at 20°C). Retinas were dissected as whole-mounts and immunostained by using a mouse monoclonal antibody to tyrosine hydroxylase (TH; 1:10,000; Sigma, St. Louis; MO) and standard streptavidin–biotin–horseradish peroxidase immunohistochemical procedures using diaminobenzidine as the chromogen. Alternatively, entire eyes were sectioned at 16 μm and similarly stained, with adjacent negative control sections being treated identically, other than the substitution of phosphate buffered saline for the primary antibody solution. All experiments were conducted under authorization by the Institutional Animal Care and Use Committee at UCSB, and in accord with the NIH Guide for the Care and Use of Laboratory Animals.

Ten retinal whole-mounts were analyzed to determine the diameter of the Type I TH-immunoreactive (dopaminergic) amacrine cells. From each retina, 100 adjacent TH-immunoreactive amacrine cells in the central retina were identified and classified as being either Type I or Type II based on their size and staining intensity (see Results section), and as residing in either the INL or the GCL. Cells were drawn by using a 100× oil immersion objective and a drawing tube, at a final magnification of 1,000×. The areas of these drawn cells were measured by using a digitizing tablet and morphometric software and then converted to diameters for circles of equivalent area (*Bioquant*; R&M Biometrics; Nashville, TN). Sections and whole-mounts of the immunolabeled retinas were photographed on a Nikon Microphot-FXA equipped with an Olympus DP-11 digital camera. The images were cropped and contrast-enhanced in Adobe Photoshop 7.0 and assembled into a photomontage in Freehand 10.0.

Data analysis

Three of the best-labeled retinas from different animals were chosen for detailed spatial analysis. The position of every individual Type I TH-immunoreactive cell in retinal whole-mounts was plotted across the entire retina by us-

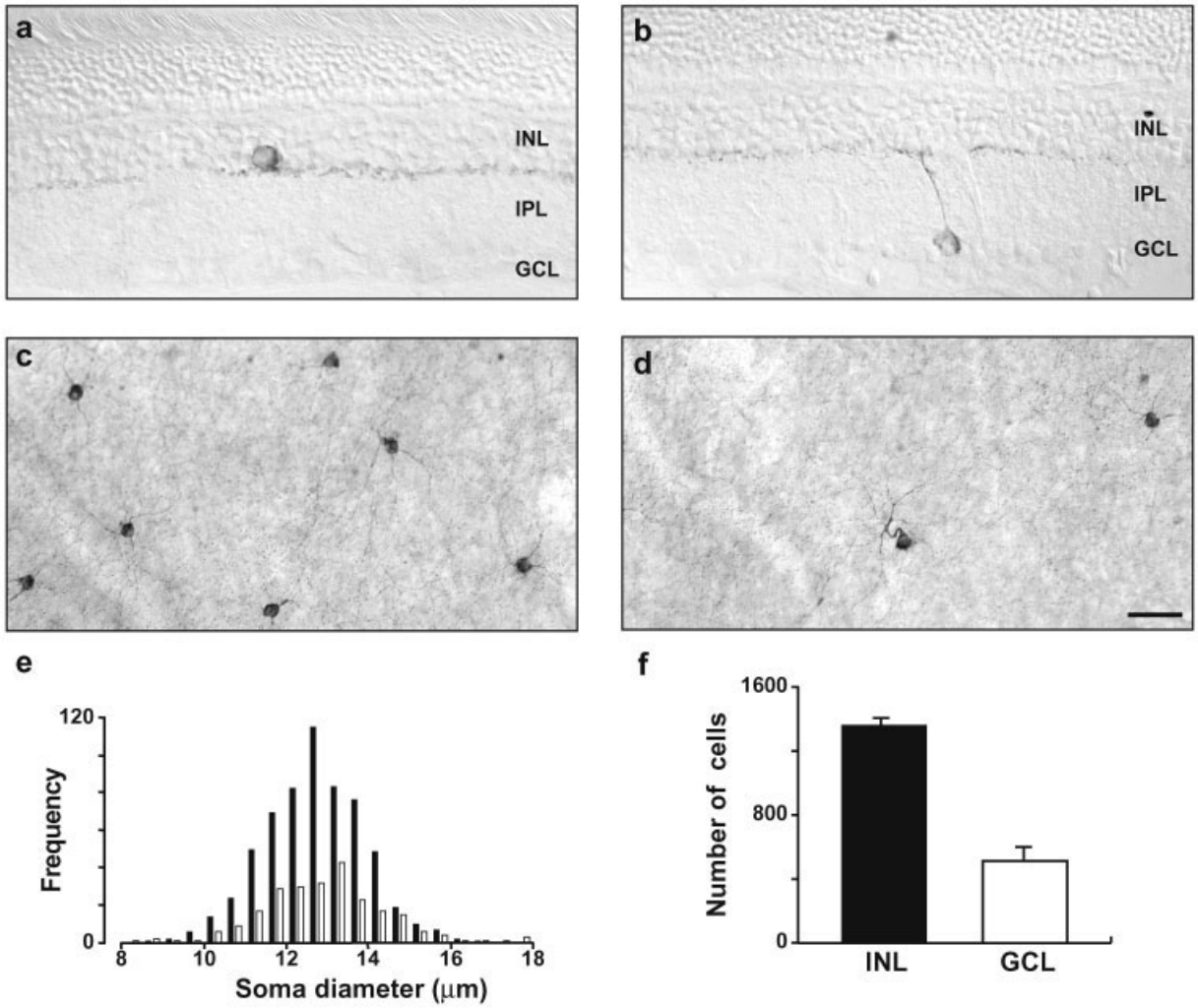

Fig. 1. **a,b**: Sectioned retinas showing dopaminergic amacrine cells positioned in the inner nuclear layer (INL; a) or ganglion cell layer (GCL; b). Cells in either layer contribute processes that stratify at the outer limit of the inner plexiform layer (IPL). **c,d**: Whole-mounted retinas showing dopaminergic amacrine cells in the INL giving rise to multiple primary dendrites in the IPL (c) or to a single primary dendrite (d) that in turn branches within the IPL, not unlike the morphology of those cells situated in the GCL (b). **e**: Soma sizes for the dopaminergic amacrine cells in the INL (filled bars) and in the GCL (open bars). **f**: Number (mean ± SD) of dopaminergic amacrine cells in the INL and GCL. Scale bar = 50 μm in d (applies to c,d); 25 μm for a,b.

ing a 40× objective and *Bioquant* topographer software. The X–Y coordinates of all cells were then exported to Excel to display their distributions and to derive one large square sample field (the largest intact field available from each retina) for further analysis, being either 2.5 mm × 2.5 mm, or 3.5 mm × 3.5 mm. Those fields were examined by using software programs customized to analyze nearest-neighbor distance and Voronoi domain area for each cell within the field (Raven and Reese, 2002). Each of these sample fields was compared with 10 random simulations matched in density. The placement of cells within those random simulations was constrained by the soma size of the real population (being 12.3 ± 1.5 μm, mean and SD; derived from the data set in Fig. 1e), effectively prohibiting two cells from overlapping one another. From these three real distributions (the INL, the GCL, and the INL+GCL populations) and each of their 10 respective random simulations, we also calculated the regularity index associated with their nearest-neighbor and Voronoi domain distributions. The regularity index is the mean nearest-neighbor distance or Voronoi domain area for a given field, divided by the standard deviation (SD), indicating the uniformity of either measure in a field (Wässle and Riemann, 1978; Raven et al., 2003). For a random distribution of cells, the nearest-neighbor regularity index has a theoretical limit of 1.91; values above this usually indicate a regular distribution of cells, although this depends on both sample size and geometry (Cook, 1996). Student's *t* tests (either two-tailed with unequal variance or paired) were performed to compare regularity indexes by using a *P* value of 0.05 for statistical significance. As we were interested in knowing whether the addition of cells in the GCL to the population in the INL improved the regularity of the mosaic, the 10 random simulations for

comparison to the INL+GCL population were each composed of the real INL population plus a random population matched in density to the GCL population.

Spatial correlograms

Spatial autocorrelograms and cross-correlograms of cell positions were computed from those three sampled fields. For each field, an autocorrelogram was produced by placing each cell at the origin and plotting the relative positions of all other cells in the field. These correlograms were then binned into annuli of constant width around the origin. The number of cells within each annulus was counted and converted into a density and then plotted as a function of annulus distance from the origin. Such a histogram is termed the density recovery profile (DRP; Rodieck, 1991). These DRPs are useful because a reduced density, or well, in the initial part of the DRP can indicate a regular distribution of cells. The size of this well can be quantified with the effective radius measure (Rodieck, 1991). Cross-correlograms were similarly created, in which each INL cell is positioned at the origin while plotting the position of all GCL cells. All DRP calculations were as described in Rodieck (1991), including the correction for border effects and the expected density for two independent Poisson processes.

Monte Carlo analysis of spatial distributions

For statistical analysis of the fields, several related spatial functions were calculated. The K function (Ripley, 1976), K(t), is the cumulative version of a DRP, but normally using smaller bin widths (4–6 μm). K(t) is the mean number of cells that are less than or equal to a distance t of a cell center, divided by the cell density. Using cumulative distribution functions reduces the impact of possible digitization errors that are introduced when setting bin widths, especially for small samples (Rodieck, 1991; Zhan and Troy, 2000). To help visually interpret the K functions, they were transformed into

$$L(t) = \sqrt{K(t)/\pi}.$$

For a Poisson process, L(t) = t and thus the L function would appear as a straight line along the leading diagonal in a graph of L plotted as a function of t. However, if the cells are regularly arranged, the L function should dip below the leading diagonal of the plot. (Conversely, if the L function appeared above the leading diagonal, the cells may be clustered.) Taking the square root of the K function also helps to stabilize sampling fluctuations (Diggle, 1986). Subscripts on K and L indicate which population of cells was used: i = INL cells; g = GCL cells; and i+g = all cells, regardless of their layer. Finally, the cross-correlation function $L_{i\times g}$ is derived from $K_{i\times g}(t)$, which measures the mean number of INL cells within distance t of a GCL cell.

To test whether a population is randomly distributed, we used the test of complete spatial randomness (CSR) from Diggle (1986). We compute the L function for an experimental field and also the L function for 99 random simulations of points in a field the same size as the experimental field. An informal test of CSR is to observe whether the experimental field falls within the envelope (min, max) of the 99 random simulations. If the L function of the experimental field falls outside the envelope, it is likely that the experimental field is not completely random. This can be quantified by using the ranking test proposed by Diggle (1986). For each field (experimental and 99 simulations), we compute a score comparing its K (e.g., K_i for the INL cells) function to the expected value for a Poisson distribution

$$u = \int_0^{t_0} (\sqrt{K_i(t)} - \sqrt{\pi t^2})^2 dt$$

The higher the value of u for the experimental field compared with the simulations, the less likely the field is random. Formally, if u for the experimental field is ranked within the top 5% of u values, we can reject a hypothesis of CSR at the 5% level. (This and the other tests proposed by Diggle [1986] are one-tailed: a low value of u indicates that the experimental field is consistent with the null hypothesis, and so we are concerned only with finding when u is much higher than u for the random simulations). The rank of the experimental field is reported as a *P* value calculated by $r/(1 + n_{sims})$, where r is the rank of the experimental field amongst the simulations (lowest score = lowest rank) and n_{sims} is the number of simulations. The integral is evaluated up to a distance t_0, which is usually 1/4 of the shortest side-length of the field.

Diggle also proposed a similar test for spatial independence between two populations of cells (Diggle, 1986). If two populations are spatially independent, we expect to find $L_{i\times g}(t) = t$. So the corresponding equation for u is

$$u = \int_0^{t_0} (\sqrt{K_{i\times g}(t)} - \sqrt{\pi t^2})^2 dt$$

In this case, as well as computing u for the INL and GCL cells of an experimental field, we generate 99 simulated fields. Each of these simulations consists of shifting all the INL cells a certain direction (chosen randomly) from their real position. Toroidal wraparound conditions are imposed so that cells remain within the observed field. If there is no spatial relationship between the two cell types, the u value for the experimental field should be similar to the u values generated by the simulated fields.

To test whether one group of cells is randomly drawn from a larger population (e.g., the minority cells in the GCL from the total population of dopaminergic amacrine cells), Diggle (1986) suggested using

$$u = \int_0^{t_0} v(t) dt$$

where v(t) is the sample variance of $\sqrt{K_i(t)}$, $\sqrt{K_g(t)}$, $\sqrt{K_{i\times g}(t)}$. Under the null hypothesis of such a random assignment, we would expect $K_i(t) = K_g(t) = K_{i\times g}(t)$, and so u increases as the K functions diverge. Again, u is computed for the experimental fields and for the 99 simulations. If N_g is the number of GCL cells, each of these simulations consists of randomly selecting N_g cells out of the total population to be GCL cells and labeling the rest as INL cells.

As another test of random assignment, we measured the effective radius from the cross-correlogram DRP of the experimental field and 999 simulations of random assignments of the field. The effective radius quantifies the volume of dead space in the central part of the auto- and cross-correlograms (Rodieck, 1991). Under the null hypothesis of random assignment, we expect the effective radius from the experimental field to be similar to the effective radii from the simulated fields. The rank of the effective radius for the experimental field among the simulated fields then determines a P value. Unlike the statistical tests from Diggle (1986), this test is two-tailed: if the null hypothesis is false, we do not predict whether the effective radius of the field will be lower or higher than the radii from the simulated fields. Hence, we reject the null hypothesis at the 5% significance level if the rank of the experimental field is < 25 ($P < 0.025$) or > 975 ($P > 0.975$) of the 1,000 possible ranks. Spatial computations were performed using the SPLANCS library and custom-purpose software written in R (Ihaka and Gentleman, 1996).

RESULTS

Size, positioning, and number of dopaminergic amacrine cells

Type I TH-immunoreactive amacrine cells, believed to be the dopaminergic amacrine cells in mammalian retina (Mariani and Hokoc, 1988; Kolb et al., 1990; Gustincich et al., 1997), have large heavily labeled somata that are most commonly found within the INL at the border with the IPL (Fig. 1a,c). These cells give rise to an elaborate spread of processes within S_1 of the IPL, emanating from a few primary dendrites (Keyser et al., 1987; Williams et al., 2001), consistent with the widefield nature of their processes described in various species (Kolb et al., 1981; Versaux-Botteri et al., 1984; Oyster et al., 1985; Savy et al., 1989; Wulle and Schnitzer, 1989; Dacey, 1990; Müller and Peichl, 1991). These cells are readily distinguished from a second class of small, faintly labeled TH-immunoreactive amacrine cells (Type II cells, thought to be catecholaminergic amacrine cells that do not use dopamine as their transmitter) which have been excluded from the present analysis (Mariani and Hokoc, 1988; Nguyen-Legros, 1988; Tauchi et al., 1990; Gustincich et al., 1997). Other Type I cells are situated within the GCL (Wang et al., 1990; Peichl, 1991), extending a single primary dendrite through the IPL to reach S_1, subsequently branching to contribute to the dense plexus at this level (Fig. 1b). Occasionally, individual cells within the INL show a single primary dendrite that arborizes some distance from the soma (Fig. 1d), as though they possessed the morphology of those in the GCL but had failed to migrate to this level or had migrated back. Those cells in the INL and GCL were not discriminable from one another on the basis of their soma diameter (Fig. 1e), averaging roughly 13 μm (t test; $P = 0.073$).

There were nearly three Type I cells in the INL (73%) for every Type I cell positioned within the GCL (27%; Fig. 1f), with the total number being 1,873 ± 160 cells (mean and SD). Their percentage in the GCL ranged from 19% to 41% (determined from samples of each retinal quadrant). Most of this variation was from sampling across the different retinas; the percentage in temporal retina was always slightly lower than in nasal retina, but those differences were minor by comparison with the interanimal variability. These Type I TH-immunoreactive amacrine cells will be referred to as dopaminergic amacrine cells hereafter.

Distribution and density of dopaminergic amacrine cells

These dopaminergic amacrine cells were found to be distributed across the retinal surface, showing little consistent variation with retinal eccentricity or retinal quadrant (Fig. 2). There was no obvious increase in density associated with the area centralis, situated in the far temporal retina in the ferret (Henderson et al., 1988). Averaged across the retinal surface, density was 22.8 ± 1.94 cells/mm^2 (mean and SD). Density was greatest in the nasal retina, averaging 30 cells/mm^2. These trends were true for both the cells in the INL and in the GCL, as well as their combined distribution (Fig. 2).

Mosaic regularity of dopaminergic amacrine cells

A single, large, square field was identified in each of these three retinal whole-mounts for analysis of the spatial geometry of dopaminergic amacrine cells. Total density in these fields was 20, 30, and 26 cells/mm^2, these samples coming from either the ventral or nasal retina. Figure 3 (left column) shows the position of each of these dopaminergic amacrine cells within the INL along with their Voronoi domain boundaries for the three sample fields A, B, and C. Likewise, Figure 3 (middle column) shows the position and Voronoi domains of dopaminergic cells within the GCL. Figure 3 (right column) shows the position of both the INL and GCL populations together and their Voronoi domains associated with the combined population. By visual inspection alone, it is unclear whether any of these mosaics is randomly or nonrandomly arranged, especially for the GCL cells which are at a much lower density than the INL cells.

To quantify the regularity of each population, we computed the standard measure of mosaic order, the regularity index (mean/SD of nearest-neighbor distances; Wässle and Riemann, 1978). Figure 4a (left and middle paired histograms) plots the mean regularity index (and SD) of the INL and GCL cells (filled bars), together with the regularity index for the 30 random simulations of equivalent density (open bars). Although in both cases the regularity index of the fields is higher than the random simulations, these differences were not statistically significant (t test; $P = 0.166$ and 0.281, respectively). By contrast, when we examined the regularity index based on Voronoi domain analysis (Fig. 4b), we found the INL population to be more regular than random ($P = 0.009$), but not the GCL population ($P = 0.104$). These results suggest, by either measure of regularity, that the GCL population is random. However, depending on whether we calculate the regularity index by using the data derived from the nearest-neighbor analysis or the Voronoi domain analysis, we might conclude that the INL cells are randomly or regularly distributed, respectively. We believe that the index based on Voronoi domain areas is a more natural measure of regularity, because it depends on the positioning of several neighboring cells and not merely the distance to the nearest neighbor (see also Raven et al., 2003). Hence, we suggest that the dopaminergic amacrine cell

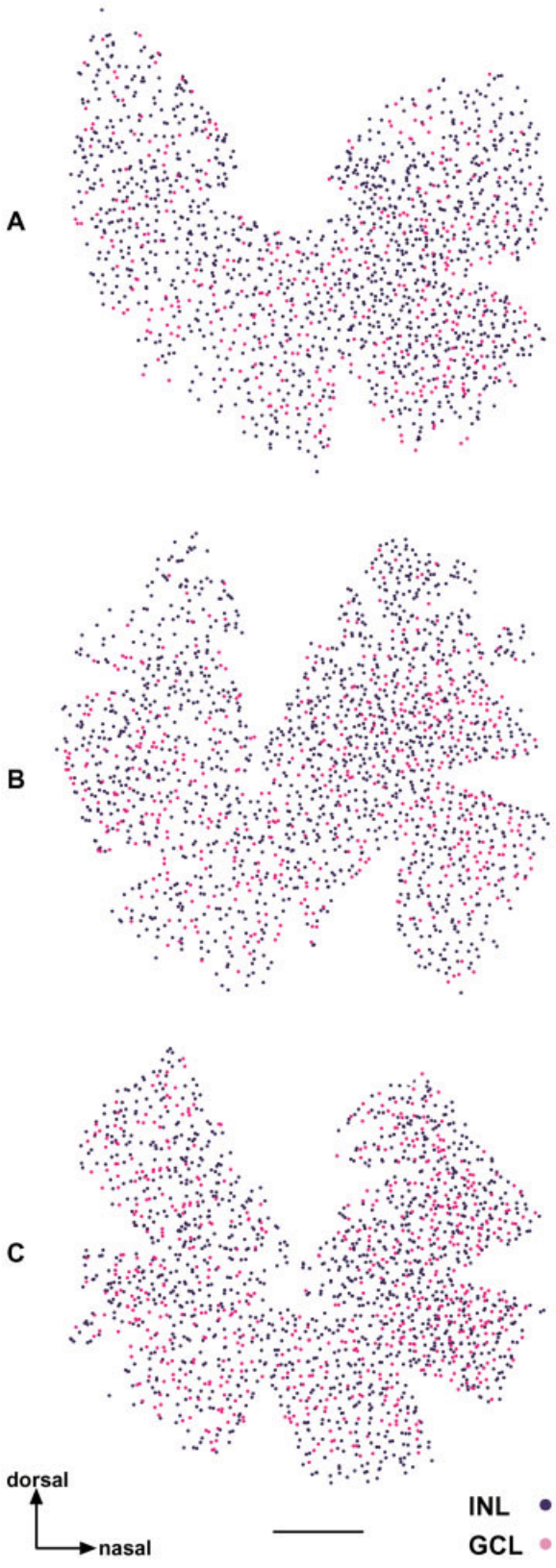

Fig. 2. **A–C**: Distribution of dopaminergic amacrine cells in the inner nuclear layer (INL) and ganglion cell layer (GCL) across the entire retina from three different ferrets. Scale bar = 2 mm.

mosaic in the INL is not randomly distributed, although it does not approximate the regularity typical of other retinal mosaics in mammalian retina for which their indexes climb to 4–6 (Wässle and Riemann, 1978; Cook, 1996).

Given that these populations have similar soma sizes (Fig. 1e), that they stratify in the same depth within the IPL (Fig. 1a,b), and that they have similar morphologies (Fig. 1a–d), those in the GCL may simply be displaced relative to those in the INL. If they together comprise a single population of cells executing the same function, then one would expect their combined mosaic (Fig. 3, right column) to be more regular than either alone. Figure 4a and b (right plots, filled bars) show the regularity indexes for the combined populations, indicating that the addition of the GCL cells to the INL cells appears to improve the regularity of the mosaic (compare the regularity index for the real INL population with the real INL+GCL population—that is, the filled bars in Fig. 4a,b, left with right plots). However, these increases in regularity were not statistically significant ($P = 0.077$ for this comparison in a, and $P = 0.158$ for it in b; because this comparison is looking at the regularity index with and without the GCL population added to the INL population, the paired t test was used).

As the GCL cells appear to be irregularly arranged, one might wonder by how much the regularity of the INL mosaic is changed by adding a random distribution of cells of the same density as that found in the GCL. Figure 4a,b indicates that the random addition of cells to the weakly regular INL mosaic serves only to degrade that mosaic further (compare Fig. 4a and b, filled bars in left histogram with open bars in right histogram), although this difference was significant only for the Voronoi analysis ($P = 0.332$ for nearest neighbor analysis; $P = 0.039$ for Voronoi domain analysis). By contrast, the combined mosaic of INL + GCL cells yielded a regularity index that was greater than that produced by randomly adding GCL cells to the real INL distribution (Fig. 4a,b, right plots, although this difference did not reach significance for the nearest-neighbor analysis either: $P = 0.077$; for the Voronoi domain analysis, $P = 0.005$). Hence, this finding would indicate that the GCL cells are not randomly positioned but just of a sufficiently low density that their distribution alone is not discriminable from a random distribution.

The results from the regularity indexes both indicate that the GCL population is not discriminable from random distributions of equivalent density, although they differ as to whether the INL population is discriminably different from random. To help resolve the issue of regularity, we used a third technique for detecting complete spatial randomness (CSR, see Materials and Methods section; Diggle, 1986). This technique has been used only rarely in the study of retinal mosaics, due to its relative complexity compared with nearest-neighbor or Voronoi methods but, together with related tests for spatial independence and random assignment (see below), has proven particularly useful for determining whether cells of similar phenotype in two different retinal layers comprise either one or two distinct populations (Diggle, 1986). Figure 5a–c shows the results of applying the CSR test to one field, that for ferret B. First, we find that the population of INL cells is not consistent with CSR, because their L function (red lines) falls outside the limits defined by the 99 random simulations (indicated by the two blue lines), i.e., they are regu-

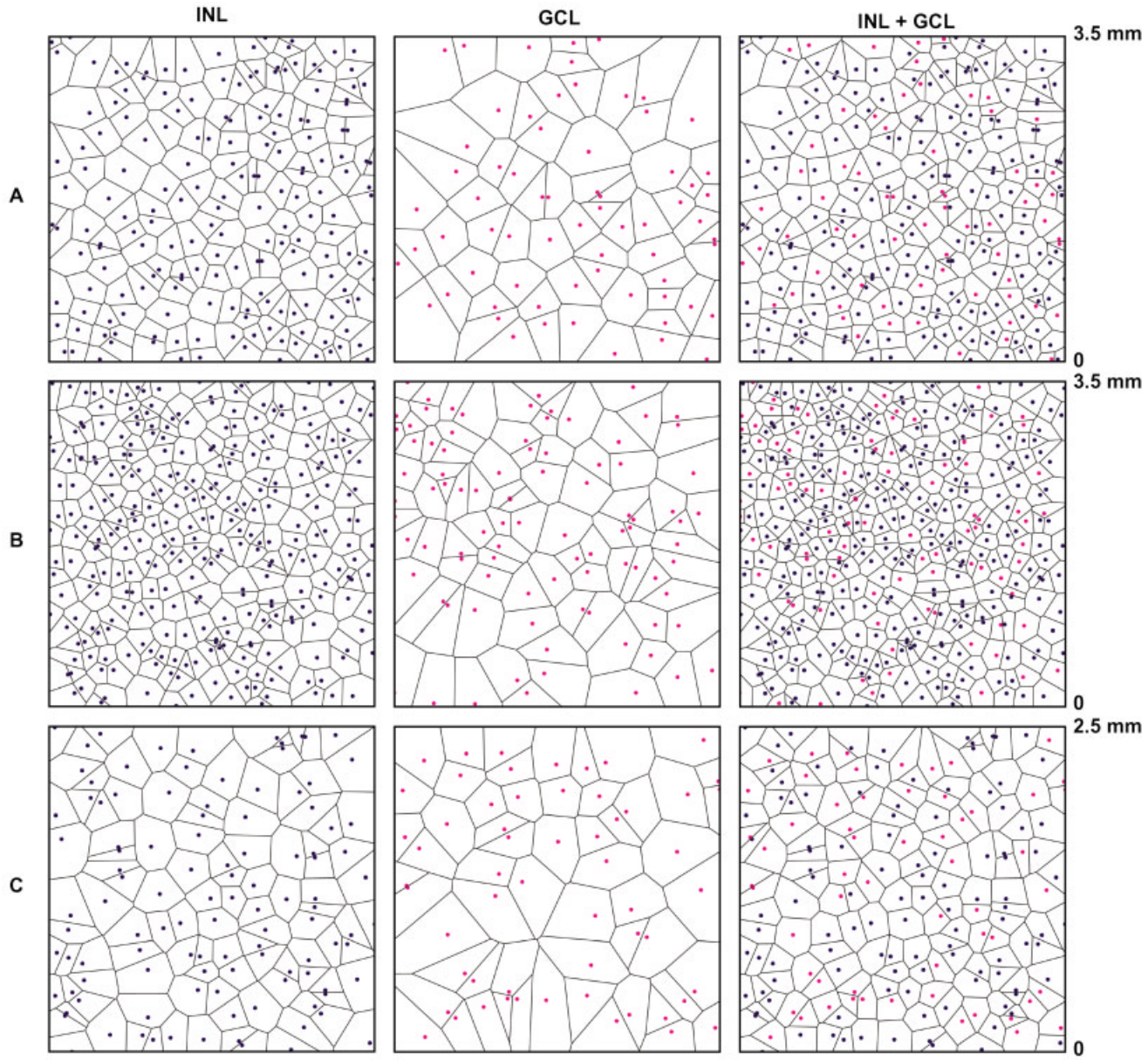

Fig. 3. Single fields of retina derived from ferrets A, B, and C in which the distribution of cells in the inner nuclear layer (INL, left column) and in the ganglion cell layer (GCL, middle column) is shown, along with their Voronoi domains. Their combined distributions, and associated Voronoi domains, are shown on the right column. Field size is indicated along the right margin. Note that the field for C was smaller than those for A and B.

lar (Fig. 5a). Second, the GCL cells, by contrast, are consistent with CSR, i.e., they appear to be arranged in a spatially random manner (Fig. 5b). Third, the combined population of cells, like those in the INL, is also not consistent with CSR; i.e., they are arranged in a regular manner (Fig. 5c).

Beneath each cumulative histogram, the rank ordering (u) of the L function for the field (red), relative to the 99 simulations (blue), is shown, from which a *P* value can be ascribed, confirming that only the GCL cells (Fig. 5b) are consistent with CSR. Similar results were found for all three fields (A, B, and C), and the *P* values associated with those L functions relative to their 99 simulated comparisons are indicated in Table 1 (tests 1–3). The results of the CSR test and the analysis of Voronoi domain regularity indexes agree, suggesting that the INL and INL+GCL mosaics are not randomly distributed. Again, the lack of regularity indicated by the index derived from nearest-neighbor distances (Fig. 4a) may simply reflect its relative insensitivity, based as it is on the positioning of only the nearest neighboring cell.

Figure 6a–c shows the average DRPs derived from the autocorrelograms from the three fields, for the cells in the INL (Fig. 6a), in the GCL (Fig. 6b), and for the combined

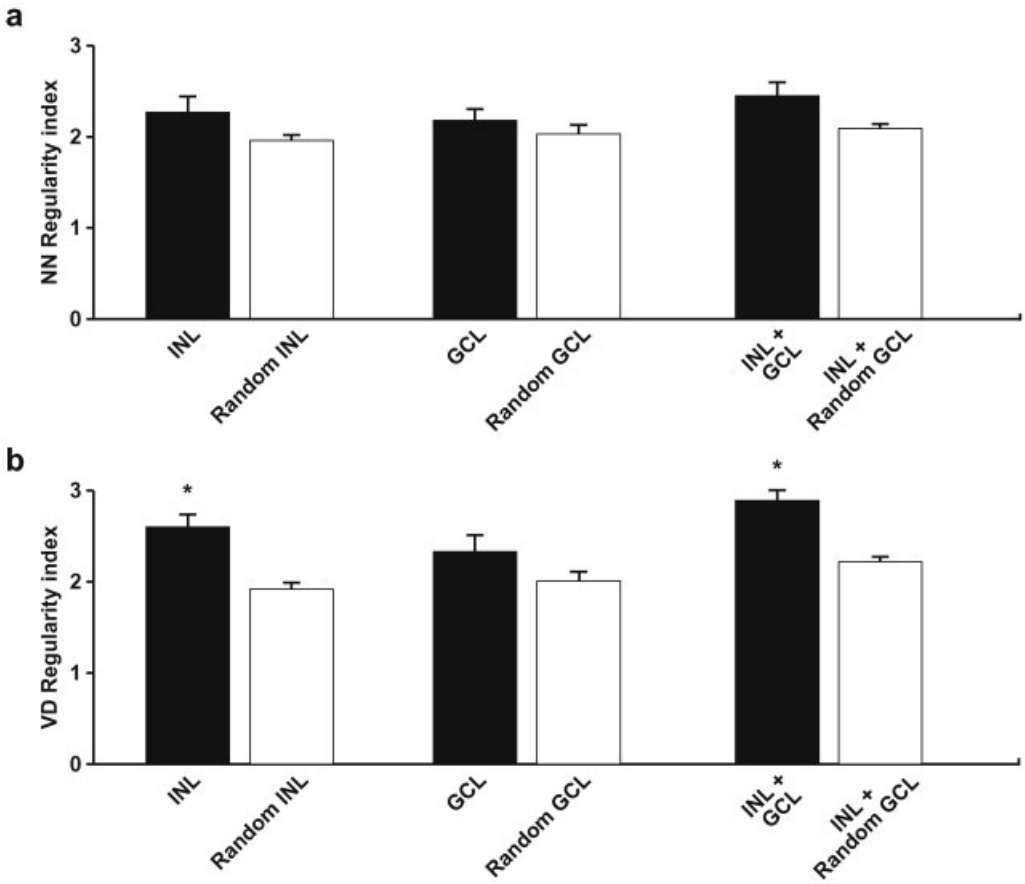

Fig. 4. **a**: Regularity indexes (mean and standard error) derived from the measurement of nearest-neighbor (NN) distances of the real data (filled bars, n = 3) and of the random simulations coupled to each real data set (open bars, n = 30). The left pair shows regularity indexes for the inner nuclear layer (INL) data, whereas the middle pair shows them for the ganglion cell layer (GCL) data. The right pair shows the regularity indexes for the combined population, and, for comparison, the regularity indexes from a field in which the real INL mosaic has added to it a random simulation of the GCL mosaic. **b**: Same comparisons of regularity indexes derived from measurement of the Voronoi domain (VD) areas. Asterisks indicate significant differences ($P < 0.05$) between the regularity indexes for the real vs. simulated mosaics.

INL+GCL population (Fig. 6c). A reduction in the density of cells in these DRPs is clearly observed in a and c, less obviously in b, up to distances of around 200 μm. Such a well in the DRP for the GCL population is obscured by the second bin which had large variance; the error bars on the DRPs are largest for the GCL cells, because these are at a much lower density than either the INL or combined population. (Note also that these correlograms and their derived DRPs were produced by using bin widths of 50 μm, much larger than used elsewhere, because of the overall lower density of dopaminergic amacrine cells.) Finally, we also computed the cross-correlogram of the INL and GCL cells and derived its DRP, finding a comparable reduction in density at these lesser distances out to 200 μm (Fig. 6d). This finding is in contrast to most previous analyses cross-correlating pairs of retinal cell types, where no spatial dependence between the two cell types was typically observed (Rodieck and Marshak, 1992; Galli-Resta et al., 1999; Rockhill et al., 2000; but see also Kouyama and Marshak, 1997; Zhan and Troy, 2000).

To test whether this well in the DRP for the cross-correlograms was significant, we used the test for spatial independence of two populations (Diggle, 1986). This tests how the $L_{i\times g}$ function varies as one population of cells is moved randomly relative to the other population of cells. If there is no spatial dependency between the two populations, the $L_{i\times g}$ for the real cell positions should look similar to $L_{i\times g}$ from the random cell populations. However, this is not the case (Fig. 5d): the L function for the real field (red line) is much lower than those generated from the random simulations, and the Monte Carlo analysis of u scores bears this out. This was also the case for the other two fields (Table 1, test 4). This analysis suggests that the well in the DRP for the cross-correlograms out to 200 μm (Fig. 6d) truly represents a spatial dependency between the two populations.

The next statistical test we applied to our data sets was the random assignment test. This test was originally described in the context of examining cholinergic amacrine cells in the INL and the GCL (Diggle, 1986). One hypothesis considered by Diggle was that all cholinergic amacrine cells are initially formed as a single mosaic, with differentiation into two subtypes occurring later in development, leading to their occupying different nuclear layers. His random assignment test considered whether each

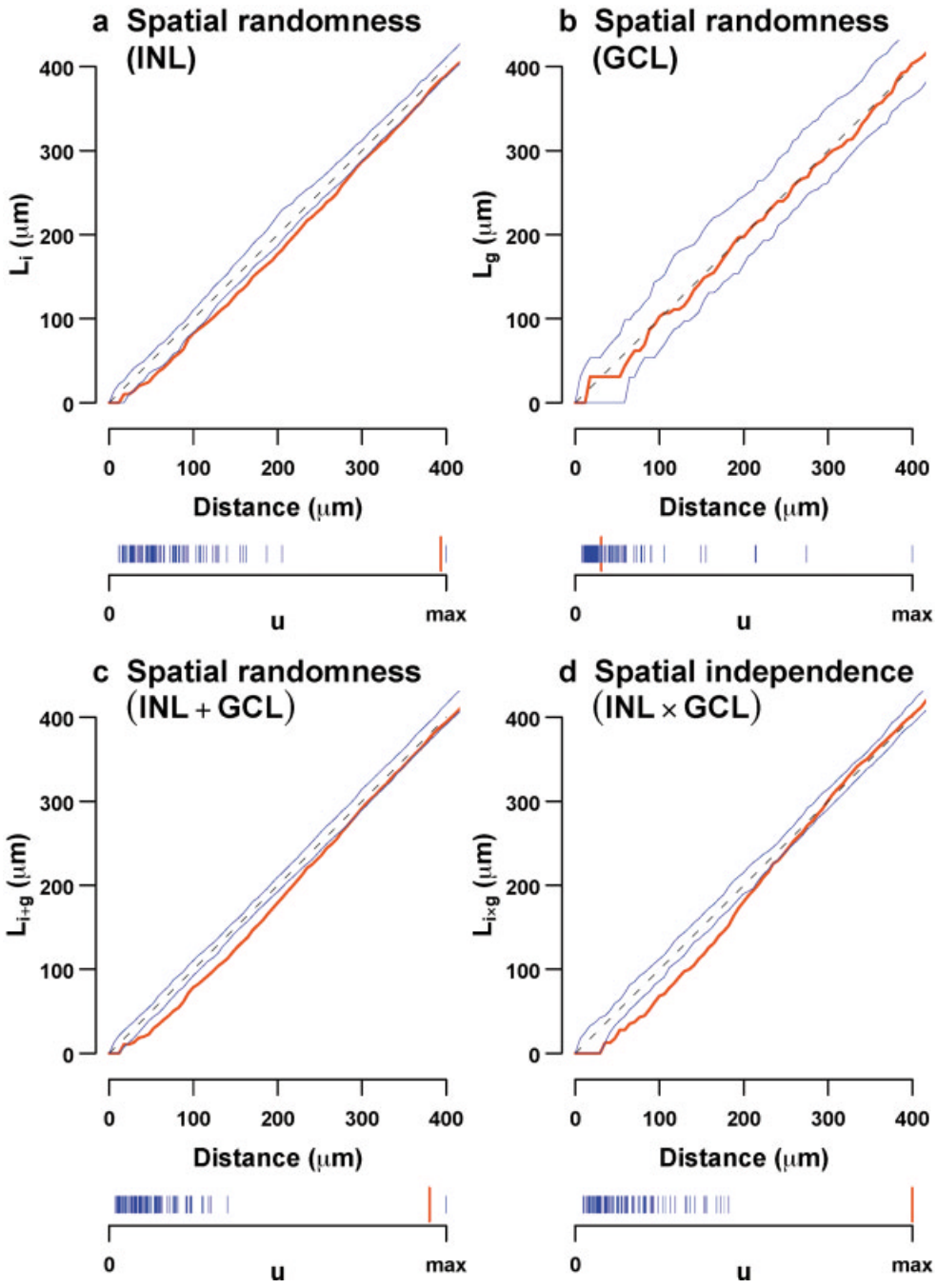

Fig. 5. Tests for complete spatial randomness (CSR) and independence of the inner nuclear layer (INL) and ganglion cell layer (GCL) cells. The layout of each subfigure is the same. In the cumulative histogram, the solid red line shows the experimental L function, and the solid blue lines are the envelope (min, max) of the 99 random simulations. The broken black line indicates L(t) = t, the theoretical value of L under the null hypothesis (CSR for a–c; spatial independence for d). The lower graph in each panel plots the ranking score, u, as a vertical line for each field: a tall red line for the experimental field, and smaller blue lines for each of the 99 simulations. Because only the ordering, not the magnitude, of each is important, each u plot is scaled to the maximum u value. **a**: Test of CSR for the INL cells. Because the experimental field falls out of the envelope of the random simulations, the INL cells are nonrandomly arranged. This conclusion is confirmed by the experimental field having a rank of u of 99 out of 100 ($P = 0.99$). **b**: Test of CSR for the GCL cells. Both visual comparison of the field with the envelope and the ranking ($P = 0.59$) indicate that the GCL population is consistent with CSR. **c**: Test of CSR for the whole population of cells. The L function again falls out of the envelope of the random simulations, consistent with the u score ranking ($P = 0.99$), and so we reject CSR. **d**: Test of spatial independence between the INL and GCL cells. Here again, the difference between the cumulative histogram for the data relative to the simulations and the u score ranking ($P = 1.00$) leads us to reject the test for spatial independence between the two populations.

TABLE 1. *P* Values Assigned by Monte Carlo Testing to Examine the Spatial Distribution of INL and GCL Cells, and Their Possible Dependencies[1]

Statistical test: null hypothesis	Field A	Field B	Field C
1. Complete spatial randomness of INL cells	1.00*	0.99*	0.95
2. Complete spatial randomness of GCL cells	0.78	0.59	0.68
3. Complete spatial randomness of INL + GCL cells	0.99*	0.99*	1.00*
4. Spatial independence of INL and GCL cells	0.97*	1.00*	1.00*
5. Random assignment of INL and GCL cells	0.53	0.78	0.82
6. Effective radius derived from random assignment	0.06	0.86	0.87

[1]Asterisks denote significant differences from the null hypothesis at the 5% level. Tests 1–5 are one-tailed, and so $P > 0.95$ for significance; test 6 is two-tailed, and so $P < 0.025$ or $P > 0.975$ for significance at the 5% level. Tests 1–3 examine whether the INL cells, GCL cells, or combined INL + GCL cells, are randomly arranged. The GCL cells alone were found to be consistent with a random arrangement, while the INL cells and the INL + GCL cells were found to be regularly arranged. Test 4 examines whether INL cell positioning is spatially independent of cells in the GCL; for each field, we found that the INL and GCL cells are spatially dependent. Test 5 examines the possibility that an initial population randomly divides into the INL and GCL population; the low *P* values indicate that this hypothesis cannot be rejected. Finally, test 6 shows that the size of the effective radius in the cross-correlograms is consistent with random assignment of cells to either the INL or GCL. INL, inner nuclear layer; GCL, ganglion cell layer.

cell independently (and randomly) decides its laminar fate from within such an initial mosaic. We applied this test to our data sets to examine whether the INL and GCL cells have subdivided from some initial population of cells. Here, one simulation consists of fixing the positions of the cells to be the same as the experimental data set, but independently randomly labeling each cell to be either an INL or GCL cell, respecting the relative number of INL and GCL cells in the experimental fields. For this test, the metric for a field (simulated or real) was the variance of each of $\sqrt{K_i}$, $\sqrt{K_g}$, $\sqrt{K_{i\times g}}$. The ranking of each of the three experimental fields against their random simulations showed that each field was consistent with random assignment (Table 1, test 5). These results, therefore, suggest that the dopaminergic amacrine cells in the INL and GCL initially form a single, modestly regular, array, before a certain proportion of cells become displaced to the GCL. According to this hypothesis, those cells should bear no particular spatial

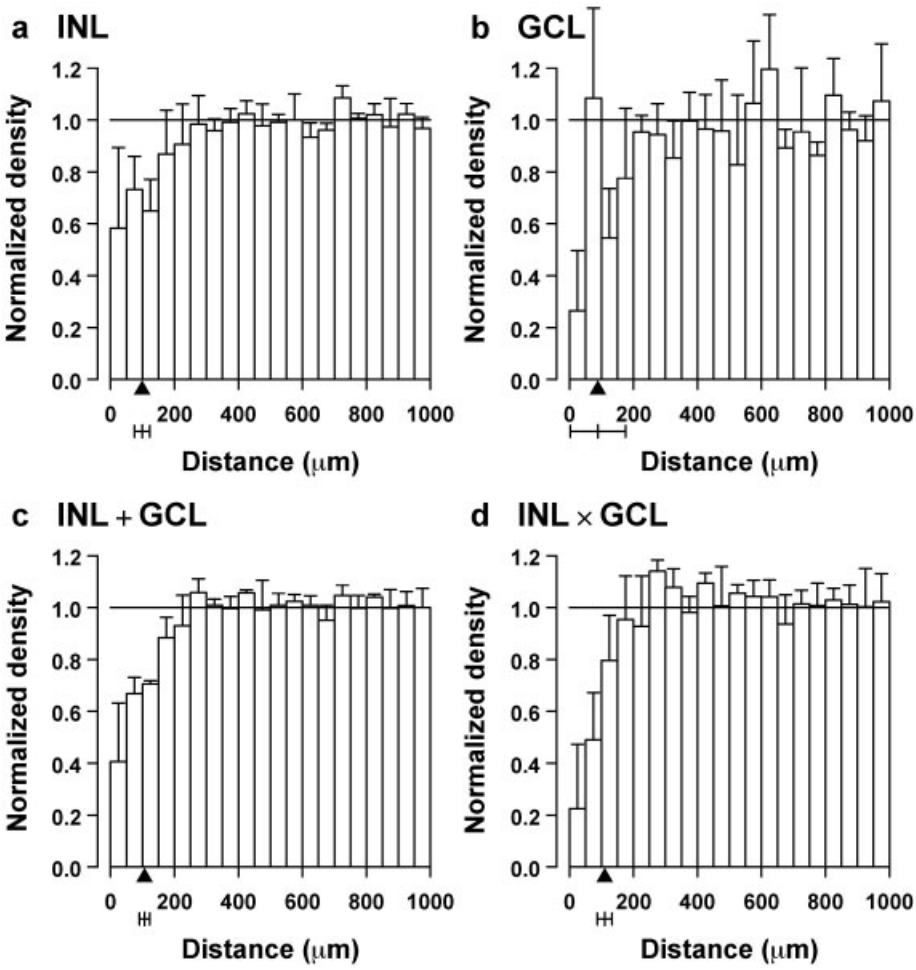

Fig. 6. Average density recovery profiles (DRPs) of the sample fields shown in Figure 3. Each bin shows the mean (and standard deviation) derived from the three DRPs associated with those fields. Bin width, 50 μm. Before averaging, each DRP was normalized such that its mean density was 1.0 (indicated by the horizontal bar at the top of each plot), to account for different densities across samples. The arrowhead beneath each DRP denotes the mean effective radius, and this mean and its standard deviation are indicated beneath the arrowhead. **a**: Mean DRP of the autocorrelation of cells in the inner nuclear layer (INL). **b**: Mean DRP of the autocorrelation of cells in the ganglion cell layer (GCL). **c**: Mean DRP of the autocorrelation of all cells, irrespective of layer. **d**: Mean DRP of the cross-correlation of the INL cells with the GCL cells. Note that the effective radius is similar in all four conditions.

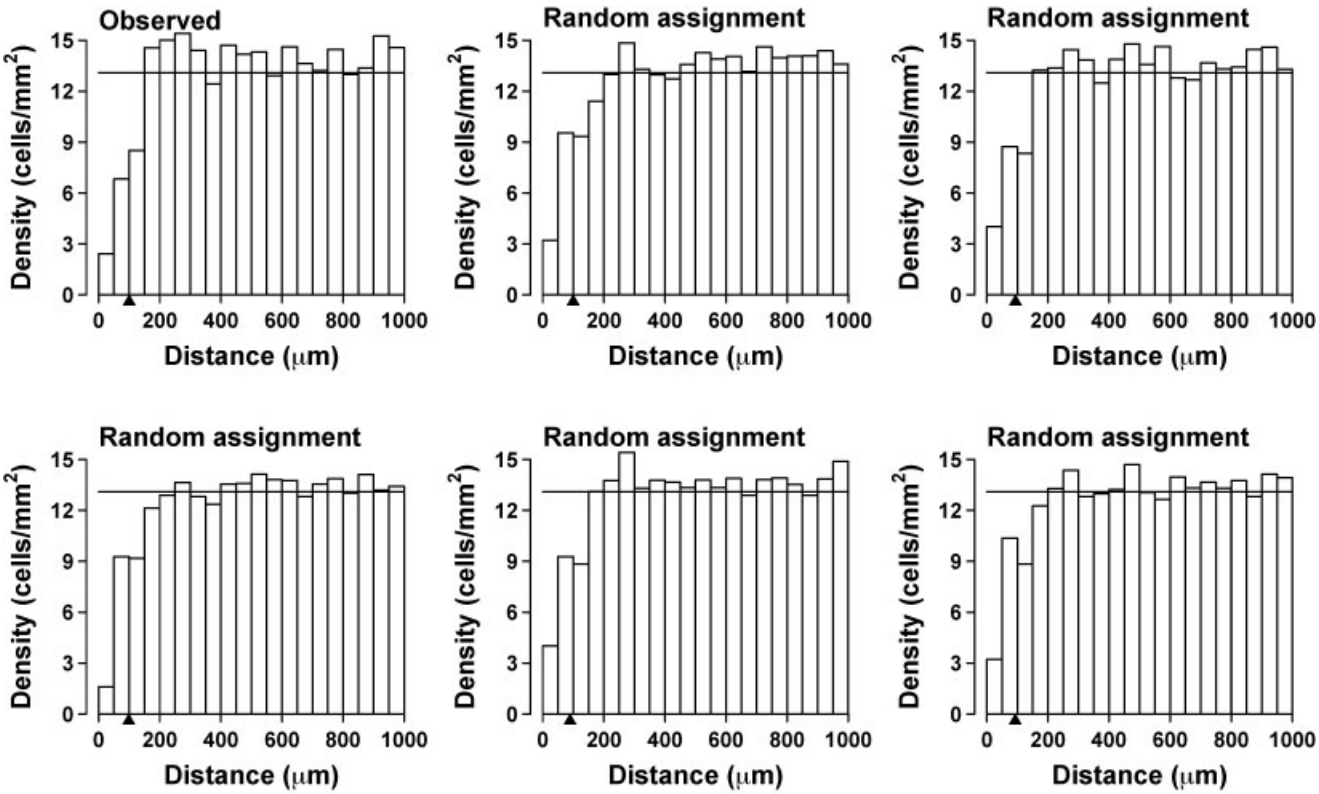

Fig. 7. Density recovery profiles (DRPs) of the cross-correlation between cells in the inner nuclear layer (INL) and ganglion cell layer (GCL) for field B. Conventions as in Figure 6, except that, because each DRP represents a single field, there are no error bars and each bin is not normalized. The top-left DRP is calculated from the experimental data; the remaining DRPs are computed after randomly assigning each cell in field B to either the INL or GCL in their normal proportion. Notice the similarity in the size of the effective radius in all six DRPs, suggesting that those occupying the GCL in the real fields in Figure 3 are randomly drawn from an otherwise homogeneous population of dopaminergic cells.

relationship to the INL cells relative to a completely random assignment of some 27% of the cells from the initial population of all cells.

To test further this hypothesis, we took the entire population of cells in each of the three experimental fields (A, B, and C), and randomly labeled the cells as either INL or GCL cells, respecting the ratio of INL to GCL cells, and plotted their cross-correlograms. Figure 7 (top left) shows the DRP of the real data derived from field B, whereas the other five DRPs (randomly selected from a total now of 999 simulations) are derived from these random assignments of INL or GCL status. Each of the random cross-correlograms in Figure 7 exhibited the same sized "well" as shown for the real data. We can objectively compare these by computing the effective radius for each of these 999 simulations, as well as for the real data (indicated by the arrowheads beneath each DRP in Fig. 7), and verify that the P values do not discriminate the real data from the randomly assigned mosaics. In each case, the ranking of the experimental field was within the central 95% confidence interval from the simulations (Table 1, test 6). This finding supports the notion that the factors determining whether a cell is to reside in the INL or GCL are operating randomly within the total population.

DISCUSSION

In this study, we show that although dopaminergic amacrine cells in the ferret are found in both the INL and the GCL, they should be regarded as one functional population. This conclusion is based on the cross-correlation analysis of cell position between the two layers. Furthermore, based on computer simulations, we suggest that the spatial distribution of cells in the INL and GCL is consistent with each cell being randomly determined, independent of the other cells, to reside in the INL or GCL.

Support for this hypothesis also comes from examining the size of the effective radius from the autocorrelograms of each field (Fig. 6). In each case, the effective radius is around 100 μm. (The variance is largest for the effective radius for the GCL cells, again because of the lower density of GCL cells compared with INL cells.) Previous work has shown that the effective radius is robust to random undersampling of a population of cells (e.g., Fig. 9b of Cook, 1996). Only when the mosaic is severely undersampled (typically leaving less than 30–40% of cells) does the effective radius start to increase. Hence, our result that the effective radius is similar across three autocorrelograms is to be expected if the INL and GCL cells are both randomly chosen from some initial INL+GCL population. Data from Cook (1996) also explain why the regularity

index of the INL mosaic is higher than the GCL mosaic but not much higher when the two are added together: the regularity index decreases sharply as a mosaic is undersampled (see Fig. 9c in Cook, 1996).

These results of a spatial dependency between the INL and GCL cells are in contrast to most previous work testing for cross-correlations between cells in the retina. A recent comprehensive study found no evidence for cross-correlations between six types of neuron in adult rabbit retina (Rockhill et al., 2000). In particular, they found no spatial correlation between the cholinergic amacrine cells in the INL and GCL, in agreement with the earlier work by Diggle (1986) where most of the statistical methodology used in our study was first described. Because these cholinergic amacrine cells also have dendrites that ramify in different sublaminae of the IPL, there is little doubt that they are in fact independent functional types. By contrast, the dopaminergic amacrine cells in both the INL and GCL position their dendrites in the same sublamina within the IPL, strongly suggestive of a functional commonality. The present results solidify this view, because their positioning relative to one another indicates a single spatial pattern from which both populations are drawn.

Developmentally, these results suggest that a single population of dopaminergic amacrine cells is produced, from which a subset is randomly chosen to migrate further vertically into the GCL. One would like to know the mechanism(s) by which the initial population of cells is constrained to form a mildly regular array. One hypothesis is that retinal mosaics are formed by lateral dispersion of neighboring cells as they interact with one another (Reese et al., 1995, 1999), perhaps mediated by homotypic dendritic interactions (Galli-Resta, 2000; Galli-Resta et al., 2002). However, dopaminergic amacrine cells, at least in the mouse, do not undergo much tangential migration (Reese et al., 1999; Raven et al., 2003). Instead, feedback inhibition might prevent neighboring cells surrounding each dopaminergic amacrine cell from acquiring the same fate, suggested in the larval frog retina (Reh and Tully, 1986). This mechanism is unlikely to be universal, however, because *bcl-2*–overexpressing mouse retinas contain many dopaminergic amacrine cell somas in close proximity, indeed, as many as would be expected from a random distribution (Raven et al., 2003). Alternatively, a regular distribution of dopaminergic amacrine cells might emerge from a random population by a process of cell death, because there is thought to be massive cell death amongst the dopaminergic cells (Strettoi and Volpini, 2002) and the cell death would only need to be weakly directed to transform a random into a regular population (Eglen and Willshaw, 2002; Raven et al., 2003).

The present results also raise the issue of the determinants of positional depth for dopaminergic amacrine cells. As these cells are positioned at only one of two levels, rather than showing the variable positioning typical of some ganglion cell classes throughout the IPL and GCL in fish retina (Cook and Becker, 1991), they clearly distinguish the cellular from plexiform layers. They are, perhaps, more like horizontal cells that are misplaced to the ganglion cell layer (Silveira et al., 1989; Wässle et al., 2000). But it is still unclear as to whether an initial array of cells first settles within the INL from which a subset then migrates into the GCL, or whether radially migrating cells simply cease their migration at two different depths. The percentage of dopaminergic amacrine cells situated in the GCL is known to vary among species. For example, less than 1% is positioned in the GCL of the rat's retina (Martin-Martinelli et al., 1994), whereas around 40% are so positioned in the dog's retina (Peichl, 1991). Indeed, within the dog's retina, their proportion varies across the retina from 10% to 85%, with no consistent pattern (Peichl, 1991). This variability across and within species is consistent with the view that a single functional population exists and that the spatial constraints imposed upon these cells as they migrate radially are more loosely controlled in some species than others, but still does not shed light on the above questions.

Even though we find that the mosaic regularity is highest (Fig. 4) when we consider the combined INL+GCL mosaic, the nearest-neighbor regularity index is still very modest (~2.43) compared with other retinal mosaics (e.g., ~4 for cholinergic amacrine cells, Galli-Resta and Novelli, 2000; ~5 for horizontal cells, Raven and Reese, 2002). Clearly, dopaminergic cells are nonrandomly arranged, but their mosaics are not precise. This finding may reflect their modulatory role in visual processing, rather than relaying any spatial features in the pattern of photoreceptor excitation, and is consistent with the extensive yet irregular spread of their processes coupled with their substantial overlap (Voigt and Wässle, 1987; Dacey, 1990). Neither the positioning of these cells in the plane of the retina, nor their positioning within its depth, appears to be regulated as precisely as found for other cells that transmit the spatial relationships contained within the visual image.

In summary, our results show that the dopaminergic cells in the INL and GCL are not independent functional types but, instead, should be regarded as a single functional type, whose cell bodies form a modest tiling of the retina when they are considered together. While this conclusion may be expected given their similar morphologies and stratification, the present results provide an objective means of advancing this view. Furthermore, we suggest that the decision for a dopaminergic amacrine cell to locate itself in either the INL or GCL is made probabilistically. Subtle variations in the environment may be sufficient to enable some number to move into the GCL, although the nature of those environmental events is unclear at this stage. Although some amacrine cell types situated in the GCL do comprise independent classes, this is not the case for the dopaminergic amacrine cells—those situated in the GCL appear to be misplaced.

ACKNOWLEDGMENTS

We thank Jeremy Cook, Dina Kronhaus, and Rachel Wong for various constructive comments on the article.

LITERATURE CITED

Brandon C. 1987. Cholinergic neurons in the rabbit retina: dendritic branching and ultrastructural connectivity. Brain Res 426:119–130.

Brecha NC, Oyster CW, Takahashi ES. 1984. Identification and characterization of tyrosine hydroxylase immunoreactive amacrine cells. Invest Ophthalmol Vis Sci 25:66–70.

Cook JE. 1996. Spatial properties of retinal mosaics: an empirical evaluation of some existing measures Vis Neurosci 13:15–30.

Cook JE. 1998. Getting to grips with neuronal diversity: what *is* a neuronal type? In: Chalupa L, Finlay B, editors. Development and organization of the retina. New York: Plenum Press. p 91–120.

Cook JE, Becker DL. 1991. Regular mosaics of large displaced and non-

displaced ganglion cells in the retina of a cichlid fish. J Comp Neurol 306:668–684.

Dacey DM. 1990. The dopaminergic amacrine cell. J Comp Neurol 301: 461–489.

Daw NW, Jensen RJ, Brunken WJ. 1990. Rod pathways in mammalian retinae TINS 13:110–115.

Diggle PJ. 1986. Displaced amacrine cells in the retina of a rabbit: analysis of a bivariate spatial point pattern. J Neurosci Methods 18:115–125.

Eglen SJ, Willshaw DJ. 2002. Influence of cell fate mechanisms upon retinal mosaic formation: a modelling study. Development 129:5399–5408.

Famiglietti EV, Tumosa N. 1987. Immunocytochemical staining of cholinergic amacrine cells in rabbit retina Brain Res 413:398–403.

Galli-Resta L. 2000. Local, possibly contact-mediated signalling restricted to homotypic neurons controls the regular spacing of cells within the cholinergic arrays in the developing rodent retina. Development 127: 1509–1516.

Galli-Resta L, Novelli E. 2000. The effects of natural cell loss on the regularity of the retinal cholinergic arrays. J Neurosci 20:RC60.

Galli-Resta L, Novelli E, Kryger Z, Jacobs GH, Reese BE. 1999. Modelling the mosaic organization of rod and cone photoreceptors with a minimal-spacing rule. Eur J Neurosci 11:1461–1469.

Galli-Resta L, Novelli E, Viegi A. 2002. Dynamic microtubule-dependent interactions position homotypic neurones in regular monolayered arrays during retinal development Development 129:3803–3814.

Gustincich S, Feigenspan A, Wu DK, Koopman LJ, Raviola E. 1997. Control of dopaminergic release in the retina: a transgenic approach to neural networks. Neuron 18:723–736.

Henderson Z, Finlay BL, Wikler KC. 1988. Development of ganglion cell topography in ferret retina. J Neurosci 8:1194–1205.

Ihaka R, Gentleman R. 1996. R: a language for data analysis and graphics. J Comput Graph Stat 5:299–314.

Keyser KT, Karten HJ, Katz B, Bohn MC. 1987. Catecholaminergic horizontal and amacrine cells in the ferret retina. J Neurosci 7:3996–4004.

Kolb H, Nelson R, Mariani A. 1981. Amacrine cells, bipolar cells and ganglion cells of the cat retina. Vision Res 21:1081–1114.

Kolb H, Cuenca N, Wang H-H, Dekorver L. 1990. The synaptic organization of the dopaminergic amacrine cell in the cat retina. J Neurocytol 19:343–366.

Kouyama N, Marshak DW. 1997. The topographical relationship between two neuronal mosaics in the short wavelength-sensitive system of the primate retina. Vis Neurosci 14:159–167.

Mariani AP, Hokoc JN. 1988. Two types of tyrosine hydroxylase-immunoreactive amacrine cell in the rhesus monkey retina. J Comp Neurol 276:81–91.

Mariani AP, Kolb H, Nelson R. 1984. Dopamine-containing amacrine cells of rhesus monkey retina parallel rods in spatial distribution. Brain Res 322:1–7.

Martin-Martinelli E, Savy C, Nguyen-Legros J. 1994. Morphometry and distribution of displaced dopaminergic cells in rat retina. Brain Res Bull 34:467–482.

Masland RH, Mills JW. 1979. Autoradiographic identification of acetylcholine in the rabbit retina. J Cell Biol 83:159–178.

Mitrofanis J, Vigny A, Stone J. 1988. Distribution of catecholaminergic cells in the retina of the rat, guinea pig, cat, and rabbit: independence from ganglion cell distribution. J Comp Neurol 267:1–14.

Müller B, Peichl L. 1991. Morphology and distribution of catecholaminergic amacrine cells in the cone-dominated tree shrew retina. J Comp Neurol 308:91–102.

Nguyen-Legros J. 1988. Morphology and distribution of catecholamine-neurons in mammalian retina. Prog Retinal Res 7:113–147.

Nguyen-Legros J, Versaux-Botteri C, Vernier P. 1999. Dopamine receptor localization in the mammalian retina. Mol Neurobiol 19:181–204.

Oyster CW, Takahashi ES, Cillufo M, Brecha N. 1985. Morphology and distribution of tyrosine hydroxylase-like immunoreactive neurons in the cat retina. Proc Natl Acad Sci U S A 82:6335–6339.

Peichl L. 1991. Catecholaminergic amacrine cells in the dog and wolf retina. Vis Neurosci 7:575–587.

Pourcho RG, Osman K. 1986. Cytochemical identification of cholinergic amacrine cells in cat retina. J Comp Neurol 247:497–504.

Puopolo M, Hochstetler SE, Gustincich S, Wightman RM, Raviola E. 2001. Extrasynaptic release of dopamine in a retinal neuron: activity dependence and transmitter modulation. Neuron 30:211–225.

Raven MA, Reese BE. 2002. Horizontal cell density and mosaic regularity in pigmented and albino mouse retina. J Comp Neurol 454:168–176.

Raven MA, Eglen SJ, Ohab JJ, Reese BE. 2003. Determinants of the exclusion zone in dopaminergic amacrine cell mosaics. J Comp Neurol 461:123–136.

Reese BE, Harvey AR, Tan S-S. 1995. Radial and tangential dispersion patterns in the mouse retina are cell-class specific. Proc Natl Acad Sci U S A 92:2494–2498.

Reese BE, Necessary BD, Tam PPL, Faulkner-Jones B, Tan S-S. 1999. Clonal expansion and cell dispersion in the developing mouse retina. Eur J Neurosci 11:2965–2978.

Reh TA, Tully T. 1986. Regulation of tyrosine hydroxylase-containing amacrine cell number in larval frog retina. Dev Biol 114:463–469.

Ripley BD. 1976. The second-order analysis of stationary point processes. J Appl Probab 13:255–266.

Rockhill RL, Euler T, Masland RH. 2000. Spatial order within but not between types of retinal neurons. Proc Natl Acad Sci U S A 97:2303–2307.

Rodieck RW. 1991. The density recovery profile: a method for the analysis of points in the plane applicable to retinal studies. Vis Neurosci 6:95–111.

Rodieck RW, Marshak DW. 1992. Spatial density and distribution of choline acetyltransferase immunoreactive cells in human, macaque, and baboon retinas. J Comp Neurol 321:46–64.

Savy C, Yelnik J, Martin-Martinelli E, Karpouzas I, Nguyen-Legros J. 1989. Distribution and spatial geometry of dopamine interplexiform cells in the rat retina. I. Developing retina. J Comp Neurol 289:99–110.

Schmidt M, Wässle H, Humphrey M. 1985. Number and distribution of putative cholinergic amacrine cells in cat retina. Neurosci Lett 59:235–240.

Silveira LCL, Yamade ES, Picanço-Diniz CW. 1989. Displaced horizontal cells and biplexiform horizontal cells in the mammalian retina. Vis Neurosci 3:483–488.

Strettoi E, Volpini M. 2002. Retinal organization in the bcl-2-overexpressing transgenic mouse. J Comp Neurol 446:1–10.

Tauchi M, Madigan NK, Masland RH. 1990. Shapes and distributions of the catecholamine-accumulating neurons in the rabbit retina. J Comp Neurol 293:178–189.

Vaney DI, Peichl L, Boycott BB. 1981. Matching populations of amacrine cells in the inner nuclear and ganglion cell layers of the rabbit retina. J Comp Neurol 199:373–391.

Versaux-Botteri C, Nguyen-Legros J, Vigny A, Raoux N. 1984. Morphology, density and distribution of tyrosine hydroxylase-like immunoreactive cells in the retina of mice. Brain Res 301:192–197.

Veruki ML, Wässle H. 1996. Immunohistochemical localization of dopamine D_1 receptors in rat retina. Eur J Neurosci 8:2286–2297.

Voigt T. 1986. Cholinergic amacrine cells in the rat retina. J Comp Neurol 248:19–35.

Voigt T, Wässle H. 1987. Dopaminergic innervation of A II amacrine cells in mammalian retina. J Neurosci 7:4115–4128.

Wang H-H, Cuenca N, Kolb H. 1990. Development of morphological types and distribution patterns of amacrine cells immunoreactive to tyrosine hydroxylase in the cat retina. Vis Neurosci 4:159–175.

Wässle H, Riemann HJ. 1978. The mosaic of nerve cells in the mammalian retina. Proc R Soc Lond B 200:441–461.

Wässle H, Dacey DM, Haun T, Haverkamp S, Grünert U, Boycott BB. 2000. The mosaic of horizontal cells in the macaque monkey retina: with a comment on biplexiform ganglion cells. Vis Neurosci 17:591–608.

Weiler R, Pottek M, He S, Vaney DI. 2000. Modulation of coupling between retinal horizontal cells by retinoic acid and endogenous dopamine. Brain Res Rev 32:121–129.

Williams RR, Cusato K, Raven M, Reese BE. 2001. Organization of the inner retina following early elimination of the retinal ganglion cell population: effects on cell numbers and stratification patterns. Vis Neurosci 18:233–244.

Wulle I, Schnitzer J. 1989. Distribution and morphology of tyrosine hydroxylase-immunoreactive neurons in the developing mouse retina. Dev Brain Res 48:59–72.

Xin D, Bloomfield SA. 1999. Dark- and light-induced changes in coupling between horizontal cells in mammalian retina. J Comp Neurol 405:75–87.

Zhan XJ, Troy JB. 2000. Modeling cat retinal beta-cell arrays. Vis Neurosci 17:23–39.